Atmospheric Research 234 (2020) 104710

Contents lists available at ScienceDirect

Atmospheric Research

journal homepage: www.elsevier.com/locate/atmosres

Improving weather radar precipitation maps: A fuzzy logic approach

Micha Silver[b], Tal Svoray[a], Arnon Karnieli[b], Erick Fredj[c,*]

[a] Dept. of Geography and Environmental Development and Dept. of Psychology, Ben Gurion University, Israel
[b] Remote Sensing Lab, Sde Boker Campus, Ben Gurion University, Israel
[c] Jerusalem College of Technology, Jerusalem, Israel

ARTICLE INFO

Keywords:
Fuzzy logic
Precipitation
Gauges
Weather radar
Location-based

ABSTRACT

Weather radar can provide spatially explicit precipitation grids. However interference, ground clutter and various causes of attenuation introduce uncertainty into the result. Typically, rain gauge observations, recognized as a precise measure of precipitation at point locations, are used to adjust weather radar grids to obtain more accurate precipitation maps. This adjustment involves one or more of various geostatistic techniques. Yet, since gauges are sparsely located, a geostatistic approach is sometimes limited or even not applicable.

This work adopts an alternative to radar adjustment by merging location-based variables with rain grids from weather radar. Recognizing that location-based variables: elevation, slope, aspect and distance from the coast all affect precipitation, these are applied to the original weather radar grid to produce an altered precipitation distribution.

The merging procedure presented here uses fuzzy logic, whereby all variables, as well as the original radar are assigned probabilities known as membership functions (MF), then a joint membership function (JMF) combines all MFs in the fuzzy set, each multiplied by its weight, to create a precipitation probability grid. This JMF probability grid is validated with gauge observation data. We show up to 30% higher correlation coefficients between gauges and the JMF grid than between gauges and the original radar. The improved correlation results from the flexibility of fuzzy logic in transforming location-based variables to probabilities.

1. Introduction

1.1. Background

Estimating spatially distributed precipitation grids is a prerequisite to flood management and flood forecasting (Merz et al. (2014)). Hydrological models need basin-scale, spatially explicit precipitation data, among other inputs, to construct accurate flood forecasts (Todini et al. (2005)) for surface runoff management. Rain radar can produce such spatial precipitation distributions, however the challenges in calibrating and correcting for the various sources of error (detailed in Villarini et al. (2008)) create spatial and temporal uncertainty in the precipitation distribution (Cecinati et al. (2017), Krajewski and Smith, 2002). Nevertheless, the underlying motivation for research in improving precipitation maps rests in the needs of hydrological modeling and flood forecasting.

Since weather radar became an accepted source of spatially distributed rainfall (Krajewski and Smith (2002), Morin et al. (2003)), extensive research has examined adjustment procedures to merge rain gauge observations with weather radar. Gauge data are accepted as reference observations (see for example Colli et al. (2013)), but represent point locations. Such point data can adjust weather radar grids through several geostatistic methods, reviewed and evaluated by Goovaerts (2000), Berndt et al. (2014) and McKee and Binns (2016). Kriging based methods have been examined by Kebaili Bargaoui and Chebbi (2009), Adhikary et al. (2017), and Ly et al. (2013). A comparison of various kriging methods where elevation was the secondary variable was done by Carrera-Hernández and Gaskin (2007). Another unique algorithm known as Conditional Merging, developed and evaluated by Sinclair and Pegram (2005), applies multiple kriging steps to achieve successful adjustment (Kim et al. (2007)) of weather radar grids.

However the density of gauge observations, required for successful adjustment and described by Otieno et al. (2014), is often lacking. The limitation of gauge density is especially severe in third world countries (Dieulin et al. (2019) but also affects precipitation modeling in European countries, such as Paulat et al. (2008). In addition, globally the number of accurate and automated gauges is dropping (Kidd et al. (2017)), further challenging the variety of geospatial adjustment techniques above. On that background, this current work presents a method

* Corresponding author.
E-mail addresses: silverm@post.bgu.ac.il (M. Silver), tsvoray@bgu.ac.il (T. Svoray), karnieli@bgu.ac.il (A. Karnieli), fredj@jct.ac.il (E. Fredj).

https://doi.org/10.1016/j.atmosres.2019.104710
Received 5 June 2019; Received in revised form 15 September 2019; Accepted 19 October 2019
Available online 31 October 2019

to improve radar precipitation grids independently of any gauge network, using location-based variables instead.

1.2. Fuzzy logic models

Since the seminal works on fuzzy systems (Zadeh (1965) and Zadeh (1975) that modeling approach has been thoroughly debated (see i.e. Zadeh (2008) for a review and response to criticism). However over the past decades, fuzzy logic and fuzzy systems have been widely adopted in the scientific community (i.e. Guiffrida and Nagi (1998) and chapter 13 of Zimmermann (2013)). Fuzzy systems consider a range of independent variables to predict some outcome. However, unlike other models, the input variables do not have exact values, rather they present probabilities of the influence of each variable on the final outcome. These probabilities are combined in a joint membership function to predict some explicit, clear cut output.

Fuzzy logic models were applied to remote sensing as early as Foody (1996). Foody (2002) evaluated uncertainty in land-cover classification models and showed that a fuzzy logic model reduces that uncertainly. Accuracy of landcover classification from historical aerial photography was validated using fuzzy sets by Okeke and Karnieli (2006). A soil erosion model based on fuzzy logic equations was developed by Cohen et al. (2008) and shown to improve runoff and erosion predictions in both small and large scale catchments compared to another conventional model. Vegetation patches in an arid environment were modeled using fuzzy logic by Svoray et al. (2007). Multiple soil and climate variables were applied in a fuzzy set model by Svoray et al. (2008) to model biomass production. In more recent research Comber et al. (2012) performed Geographically Weighted Regression (GWR) on two land-cover data sets, one derived from classic remote sensing classification, and the other from a fuzzy logic method. They found that applying GWR to the two data sets can reduce uncertainly in a final land-cover product.

Among the early applications of fuzzy logic to weather modeling was Hundecha et al. (2001) where the rainfall-runoff relation was evaluated. Berenguer et al. (2006) examined the possibility of applying fuzzy logic to identify anomalous propagation in radar reflectance. An interesting effort by Yang et al. (2013) and an earlier conference report by Wang et al. (2012) applied fuzzy logic to weather radar to discriminate convective from stratiform storm types. Later both Krause (2016) and Dufton and Collier (2015) expanded on that work and presented methods for discriminating several non-hydrological echos in Doppler weather radar using fuzzy logic. Asklany et al. (2011) used a fuzzy system to predict rainfall events, where the inputs consisted of climate variables and the fuzzy rule base was composed of a series of if-then conditions. Additionally, Giap (2014) presented a fuzzy based method to identify faulty rain gauges. Agboola et al. (2015) developed a fuzzy logic based model to predict precipitation based on a collection of climate variables. Also in Men et al. (2017) a fuzzy clustering algorithm was developed to forecast rainfall. Finally, flood risk was modeled by Wijitkosum and Sriburi (2019) using a combined fuzzy logic and an analytical hierarchy process. They used a collection of meteorological variables, soil characteristics and anthropogenic factors.

The fuzzy set approach allows describing the independent variables as probabilities, or membership functions (MF), rather than rigid variables as in regular regression models. Advanced machine learning regression algorithms also create a best-fit model from a set of rigid variables. Interestingly, the combined fuzzy-neural network approach (Jang (1993)) has seen renewed interest (for example Besalatpour et al. (2012), Hong et al. (2018)). The fuzzy set approach incorporates flexibility in mapping the variables to a probability function that cannot be attained in a regression approach. Yet the fuzzy model result, as expressed in the joint membership function (JMF) produces a definitive, clear cut output by combining the influences of all independent variable MF probabilities.

1.3. Independent variables

Previous research applying fuzzy logic to determine precipitation (mentioned above in Section 1.2) choose meteorological variables such as temperature, humidity, or snow depth. The current work analyzes location-based variables: elevation, slope, aspect, and distance from the coast, as well as rain radar precipitation grids.

The correlation between rainfall and elevation, probably due to orographic forcing, has been well documented (for example: Goovaerts (2000), Daly et al. (1992) and Carrera-Hernández and Gaskin (2007)). Guan et al. (2005), working in a mountain region of New Mexico, applied a window surrounding rain gauges, and found high correlation between the gauge observations and elevation within the window. Lassegues (2018) researched aggregated rainfall and elevation in the western Alps with a relatively high density of gauges and applying geostatistic spatial analyses. Another recent research paper by Tang et al. (2018) reported correlation between precipitation data from the Tropical Rainfall Measuring Mission (TRMM) and elevation in the Tibetan plateau. Slope as a variable was examined by Sanchez-Moreno et al. (2014), along with elevation using 30 years of monthly aggregated rainfall data in Cape Verde. They found that, in some seasons, slope was better correlated to precipitation than elevation.

Research on precipitation and proximity to the coastline has consistently found higher rainfall levels near the coast (Hayward and Clarke (1996)). Some of this work focuses on the difference between forested and non-forested regions, for example Makarieva et al. (2009). Working with a global database of gridded monthly average precipitation, they report an exponential drop in precipitation level with distance from the coast in non-forested regions. In a different climatic region, Daniels et al. (2014) analyzed changes in precipitation in the Netherlands over a 60 year period. Their statistical analysis took into account variables such as soil type and slight changes in elevation, as well distance from the coast. They reported that the highest precipitation levels were in the first two coastal zones, up to 100 km. from the coastline. Ogino et al. (2016) examined global data from TRMM and showed sharp drops in elevation within 300 km from coastlines in tropical regions.

Weather radar has been used for decades to produce rainfall grids. Indeed, several national weather services distribute gauge adjusted radar images continuously (i.e. the German Deutcher Wetterdienst (DWD) (https://www.dwd.de/EN/ourservices/radar_products/radar_products.html) and the Royal Netherlands Meteorological Service (https://data.knmi.nl/datasets). Radar derived rain rates are affected by several sources of uncertainty (Krajewski and Smith (2002), Sebastianelli et al. (2013)), yet these data cover the region with a continuous grid of relatively high resolution (Morin et al. (2003)). Although not a location-based variable, weather radar provides the model with the crucial base precipitation grid, with which the other four variables are merged.

Aspect, defined as the compass direction of slope faces, adds to the model a component of synoptic conditions. When a storm proceeds across the study area in some distinct direction, then slopes facing the storm will experience higher rainfall (Reid (1973)). Working in the Tibetan plateau, Tang et al. (2018) compared satellite-borne rain detectors (Global Precipitation Measurement (GPM) and TRMM) to gauge observations, and also found correlation between precipitation and wind-facing slopes. In addition Guan et al. (2005) applied multivariate regression to gauge data, using terrain variables, including aspect. They reported the highest correlation to precipitation when combining elevation, aspect and atmospheric moisture.

At smaller scales, both Sternberg and Shoshany (2001) and Kadmon and Danin (1999) investigated tree and shrub biomass in a Mediterranean climate as a function of aspect, and both found that storm facing slopes had higher water availability, and thus higher biomass. Work by Arazi et al. (1997) and Sharon and Arazi (1997) analyzed the effects of wind on precipitation rates in small catchments. Similarly Sevruk and

Nevenic (1998) researched the wind-induced effects of rainfall measurements, comparing the windward versus leeward spatial distribution of precipitation. However their work focused on local, micro-topography.

A long term classification of synoptic events in the eastern Mediterranean, published in Alpert et al. (2004), was adopted in this current work to find the proportion of storm directions for each month during the study period. Using their dataset, we determined for each month what percent of storms moved into the region from each compass direction. Then the aspect grid was used to determine storm facing slopes at the pixel level. Thus, inclusion of both slope and aspect as variables in the current research added novel components to the model.

1.4. Temporal aggregation

The model and validation presented in this work refer to monthly aggregated rainfall. The limitations of correlating precipitation measurements from different sources at short time intervals has been discussed by Kirstetter et al. (2010), Marra and Morin (2018) and others. These limitations result from several spatial and temporal discrepancies between gauges and radar: gauges are point measurements while radar is represented on a grid; wind drift and the time gap between rain droplets in the clouds and rainfall on the ground cause time shifts; and the timing of radar sweeps and gauge aggregation intervals are often different. Marra and Morin (2018) examined temporal auto-correlation from one minute X-band weather radar, and showed high correlations only when data was aggregated to extended time intervals. Similarly Kirstetter et al. (2010) prepared analyses of residuals between radar and gauge observations and presented increased values for R^2, mean relative error and Nash Sutcliffe coefficients as the time interval increased. Research by Sideris et al. (2014) produced accurate adjusted rainfall grids using co-kriging of several time steps from earlier radar images. Yet even in that research the problems associated with correlation of rainfall data at small temporal resolution were raised. In the current work, both weather radar grids and gauge observations were aggregated over a month to insure that temporal resolution effects were avoided.

1.5. Objectives

This current work departs from the usual geostatistic approach described above. A spatial distribution of precipitation from weather radar is produced by applying fuzzy logic to a set of five variables: the weather radar itself, elevation, slope, aspect, and distance from coast.

The objectives of this research include:

- Use fuzzy logic to improve weather radar precipitation maps;
- Apply location-based variables to the newly developed methodology;
- Validate the precipitation maps with gauge observations at two time intervals: monthly and daily (individual storm events) aggregations;
- Highlight the advantage of the fuzzy approach in the context of weather radar precipitation.

2. Methodology

This section details the procedures to download required data, create probability raster layers for the variables described in Section 1.3 above, and prepare and analyze the final JMF. The GRASS-GIS (Neteler et al. (2012)) commands and additional python scripts will be made available on request.

2.1. Study area and data acquisition

This work focuses on two climatic zones in the eastern Mediterranean region: an arid zone in southern Israel (Köppen-Geiger classification (as in Kottek et al. (2006)) BWh and BSh), and a Mediterranean climate in the north (Köppen-Geiger CSa). The northern study area experiences annual rainfall between 400 and 900 mm/yr. The southern region, on the other hand, is semi-arid to arid, receiving only 50–250 mm/yr. Weather radar data were available from two C-band (5.6 GHz.) radar stations, near Mitzpeh Ramon in the south, and Safed in the north (see Fig. 1), covering a study period of four winter (wet season) months: January, October, November and December 2018 as well as January 2019. Raw data from these radar stations were pre-processed (using the *ωradlib* library, Heistermann et al. (2013)) as follows:

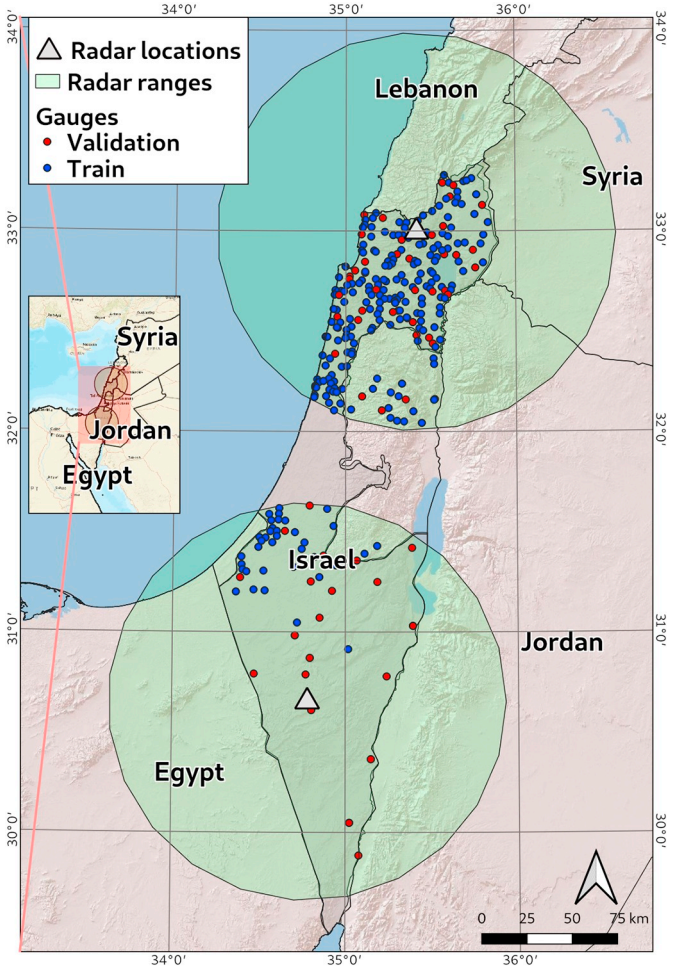

Fig. 1. Study area, radar ranges and gauge locations. The northern radar covers a region with Mediterranean climate, and the southern radar covers an arid region. Rain gauge locations are categorized as training and validation (Section 2.1).

1. Only three lower elevation angles were considered: -0.5^o, 0.9^o and 2.3^o;
2. Three corrections were applied to each individual radar file: Path Integrated Attenuation, Beam Blockage, Ground Clutter removal;
3. dBZ (from raw radar data) was converted to rainfall depth using the standard Z-R power law, Eq. (1):

$$R = \left(\frac{Z}{a}\right)^{(1/b)} \tag{1}$$

where a = 316 and b = 1.5 following arid region power law parameters in Morin and Gabella (2007);

4. The radar stations changed scan mode (sweep speed, and elevation angles) occasionally. The three scan modes were treated separately,

and data was aggregated only after applying corrections;
5. Data was aggregated by hour, day, and month;
6. A full seasonal aggregation was also prepared and used to extract range degradation parameters, using the approach in Morin and Gabella (2007) for arid regions. Linear regression slope and intercept were determined from the radar/gauge ratio compared to distance of gauges from the radar. These were then applied to each monthly aggregation to correct for range degradation.
7. A Mean Field Bias adjustment factor was determined as the quotient of mean range-corrected radar values and mean gauge values. This multiplicative factor was then applied to each monthly aggregation;
8. The original Polar coordinate system was projected and resampled to a Cartesian, georeferenced coordinate system of 1 km. resolution.

Gauge data were obtained from the Israel Meteorological Service[1] (IMS) at both monthly and daily accumulation intervals for the months of the study period. A total of 61 automatic (online) gauges contained data for these time periods: 24 in the southern and 37 in the northern study areas. Also daily aggregations were acquired for specific storm events, October 25, 2018, December 7, 2018 and January 16, 2019. Metadata, also acquired from the IMS website, contained longitude/latitude for each gauge. The aggregated monthly precipitation, once joined to the gauge metadata, created point layers of monthly aggregated observations used in this work for validation (Section 2.4).

The IMS also maintain a larger network of gauges that are manually checked each day. From personal communication, the IMS consider both sets of gauges equally reliable with data collection intervals of 10 min in both cases. This *sec*ond set of manual gauges, 266 of which fell in the two study areas, was used to determine radar correction parameters as described above. Both sets of gauges are well distributed throughout the country (as displayed on the map in Fig. 1), thus by splitting the full set of IMS gauges according to gauge type, automatic or manual, a larger set of data was used for tuning the model and radar correction, and a smaller, independent set for validation.

An elevation grid covering the study area was acquired from the Shuttle Radar Terrain Mission (SRTM) program[2] at 3 arc sec (about 90 m) resolution. In addition to serving as elevation data for the study area, this layer was also processed to produce slope and aspect grids, which became components of the fuzzy set. These elevation, slope and aspect grids were all downscaled to 1 km. resolution to match the Cartesian grid of the radar data.

2.2. Membership functions and probabilities

This work focused on location-based variables. Five variables were considered which affect precipitation:

1. Elevation;
2. Distance from the coastline;
3. Slope;
4. Aspect;
5. Rainfall from weather radar.

Having chosen the influencing variables (Section 1.3), a MF was assigned to each, thereby constructing the fuzzy set. MFs are represented by probability curves that span the range of possible values for each variable. The MF maps variable values to probabilities (with values from 0 to 1.0). Fig. 2 shows the MF probability curves for each variable. Three of the variables are static throughout the study period: elevation, slope and distance from coast. Each was represented by an "S" shaped curve (Eq. (2)) given by the exponent of a *sine* curve with two turning points p_0 and p_1 (following Klir and Yuan (1995), chapter 1 and implemented as in Jasiewicz (2011)).

$$MF = \begin{cases} 0 & v_x <= p_0 \\ \sin\left(v_x \cdot \frac{\pi}{2}\right)^2 & v_x > p_0 \text{ and } v_x \le p_1 \\ 1 & v_x > p_1 \end{cases} \quad (2)$$

where v_x is the vector of possible variable values.

The turning points, listed in Table 1, were chosen as a percent of the full range of each variable. Thus the elevation MF varies from 400 m. below sea level (the Dead Sea area) to 1000 m., the peak elevations in the northern study area. The lower turning point was chosen at 10 m., just above sea level, and the second at 330 m., a third of the maximum elevation. Thus all low elevations got precipitation probabilities near to zero. The probability then rose quickly, reaching 1.0 at elevation 400 m. The coastal plain in the study areas includes elevation to over 200 m., while 300 m. and above are mountainous. Thus the chosen turning points set low to moderate probability for the coastal plain and high probability in the mountain regions. This choice reflected past research (cited in Section 1.3) which showed the effects of elevation on precipitation.

Similarly, the slope MF varied from 0^o to a maximum of 34^o slope angles. All flat areas, up to 4^o were designated zero probability, then for moderate slopes of 4^o to 10^o probability increased rapidly, reaching 1.0 at slope above 20^o.

The distance from coast MF curve behaves inversely, with the high turning point at 50 km. and low turning point at 100 km. In this way, the coastal areas gained high probability values, whereas far to the south, the arid region dropped to zero probability. Research on the correlation between precipitation and distance from the coast (sources cited in Section 1.3) indicated that inland precipitation is affected by the sea up to a few hundred kilometers from the coast, justifying the distances chosen above.

The other two MF's varied from month to month. The radar MF reflects the aggregated monthly precipitation from radar data, thus each month had a different probability MF curve. However all monthly curves were prepared in the same way. Minimum and maximum precipitation values (R_{min} and R_{max}) were extracted from the monthly weather radar aggregation. The maximum was determined after removing outlier values, where outliers were defined as values above the 98th percentile. From visual inspection of the radar images, these outlier pixels were assumed to result from non-meteorological, high reflectance ground clutter that persisted even after ground clutter removal. Then turning points were set at $p_1 = 0.9 \cdot (R_{max} - R_{min})$ and $p_0 = 0.01 \cdot (R_{max} - R_{min})$ and the "S" curve Eq. (3) was then applied.

The resulting radar MF probability curve transformed low radar precipitation to almost zero probability, then the curve rose slowly; only the pixels with heaviest monthly aggregated rainfall were transformed to probability of 1.0. Justification for this radar MF originates from the various sources of uncertainty in weather radar that are not dependent on rainfall intensity. Villarini and Krajewski (2010) as well as Chumchean et al. (2003) and others reviewed sources of uncertainty in deriving rainfall from radar reflectance. Errors associated with beam blockage, polar-Cartesian conversion and calibration of the radar are independent of the rain intensity. Also wet radome effect and to some extent vertical profile of reflectivity do not increase in heavier storms. Thus their relative effect is greater in low intensity rain events. Overall the weather radar signal to noise ratio is low (i.e. high noise level) when rain intensity is low. At high rain intensity, the above sources of error are, to some extent, overcome by the strength of the signal received by the radar. Therefore, the radar MF was chosen to mirror this uncertainty by assigning very low probability to low rain intensity, and increasing the probability to 1.0 as the rain intensity grows towards the monthly maximum.

The aspect MF also varies by month, but was handled differently. Rather than an "S" curve, probability values were determined for each

[1] from: https://ims.data.gov.il/, in hebrew
[2] from ftp://edcsgs9.cr.usgs.gov/pub/data/srtm/version1

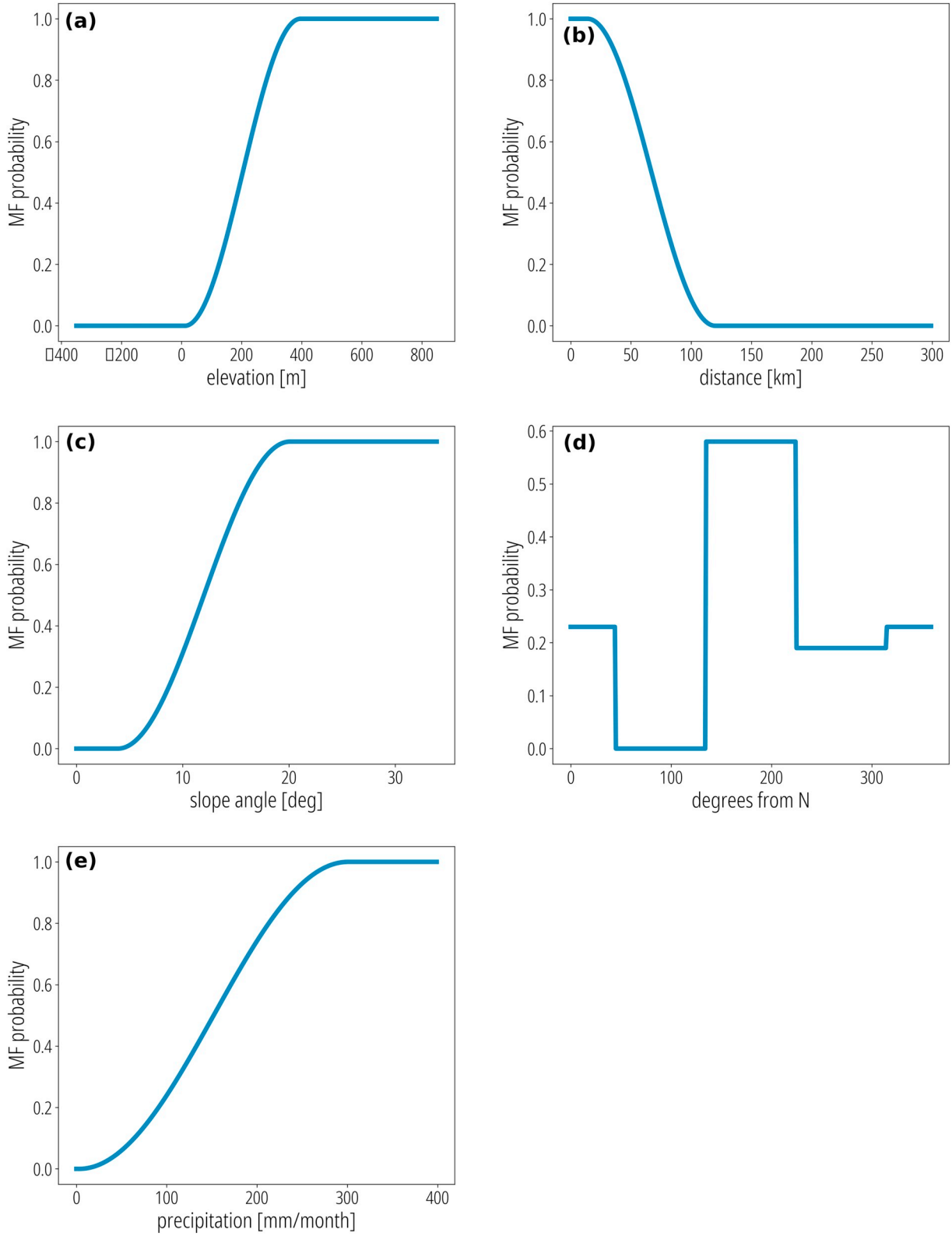

Fig. 2. Static and monthly varying membership function curves. (a) Elevation, (b) Distance from coast, (c) Slope, (d) Aspect, (e) Radar.

of the four compass directions, resulting in a rectangular probability function. The probability for each direction was derived from the proportion of the synoptic classes (see Section 1.3 and Alpert et al. (2004)) in a particular month. Referring to panel (d) in Fig. 2, which represents January, 58% of the synoptic events during that month were classified Red Sea Trough (based on data from personal communication and Alpert et al. (2004)), which moves northward. So all south facing pixels, from 135^o to 225^o were assigned a probability of 0.58. Approximately 23% of the synoptic events during January were classified as normal Cyprus Low fronts moving eastward. So west facing aspect angles of 225^o to 315^o got a probability of 0.23. In this fashion rectangular MF curves for aspect were prepared for each month.

Table 1
Turning points for each curve.

Variable	Min. value	p_0	p_1	Max. value
Elevation	−400	10	330	1000
Dist. from coast	0	50	100	220
Slope	0^o	4^o	20^o	34^o
Aspect	(rectangular function, described in the text)			
Radar	R_{min}	$0.01 \cdot (R_{max} - R_{min})$	$0.9 \cdot (R_{max} - R_{min})$	$R_{max} - R_{min}$

Table 2
Optimized weights.

Region	Radar	Elevation	Aspect	Slope	Dist. from coast
South	0.13	0.18	0.05	0.08	0.56
North	0.54	0.09	0.02	0.02	0.33

2.3. Joint membership function

In fuzzy set theory, MFs are combined using one of several types of joint membership functions (JMF): intersection, union, exclusive disjunction, or combinatorial. These types are explained in chapter 2 of Zimmermann (2013) and other textbooks on fuzzy sets. An intersection JMF finds the minimum of all MF probabilities, while a union JMF finds the maximum. Exclusive disjunction returns the probability of one MF less the inverse of the other MF. A combinatorial JMF is comprised of the sum of all MFs, each multiplied by some weight. The JMF in the current work was constructed using a combination of all MFs, by summing the products of each variable probability P_{mf} by its weight, w_{mf} as in Eq. (3). Choice of this type was dictated by the need to include all of the location-based variables in calculating the final precipitation grid.

$$JMF = \sum_{allMF} w_{mf} \cdot P_{mf} \tag{3}$$

The vector of weights was determined by performing 100 iterations of a global optimization function (using the basin hopping technique). This function calculated the correlation between gauge observations (using the set of manual gauges only) and the JMF probability at the gauge locations, and found the weights that minimized $1 - correlation$. The optimization algorithm ended after cycling through 15–25 steps with no change in the result. Weights were then normalized such that the sum of the weights equaled 1.0. The final, optimized weight vectors appear in Table 2.

Applying the JMF resulted in monthly precipitation probability grids (values from 0 to 1.0) at the same resolution and extent as the original radar precipitation grids. The authors recognize that hydrometeorological models require a high temporal resolution of precipitation grids for flood forecasting applications. Therefore, despite the difficulties producing rain grids over short time intervals, an attempt was made to apply the model to three 24 hour periods, with some

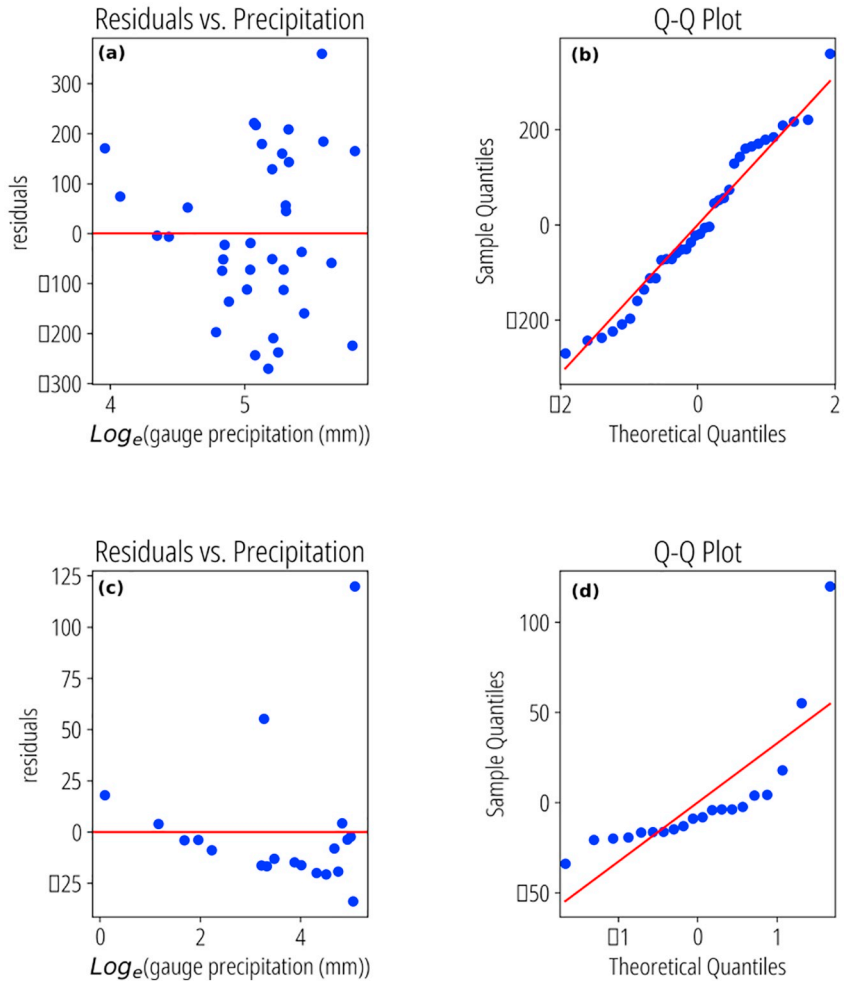

Fig. 3. Residuals tests. Residual plots show heteroscedasticity in panels (a) and (c); Q-Q plots, panels (b) and (d) show non-normality of residuals distribution. The graphs (a) and (b) refer to north study area, and panels (c) and (d) refer to south study area.

Table 3
Monthly correlation statistics: Kendall's tau between radar precipitation and gauge observations and between Joint Membership Function (JMF) and gauges.

Study area	Month	Kendall's tau		Residuals test		β coefficients	
		K-tau Radar	K-tau JMF	SW *p-value*	BP *p-value*	Slope	Intercept
North	01/2018	0.297	0.466	0.771	0.383	0.221	−0.728
North	10/2018	0.438	0.486	0.000	0.787	0.045	0.194
North	11/2018	0.641	0.610	0.825	0.479	0.110	−0.068
North	12/2018	0.152	0.533	0.906	0.142	0.169	−0.495
North	01/2019	0.162	0.406	0.307	0.313	0.079	0.005
South	01/2018	0.663	0.811	0.000	0.240	0.150	−0.136
South	10/2018	0.578	0.449	0.400	0.000	0.054	0.346
South	11/2018	0.554	0.596	0.033	0.313	0.149	−0.049
South	12/2018	0.406	0.765	0.099	0.022	0.134	0.124
South	01/2019	0.650	0.564	0.069	0.022	0.057	0.426

The Residuals test columns show Shapiro-Wilk (SW) and Breusch-Pagan (BP) test for heteroscedasticity, where **bold numbers** emphasize low *p-values*, indicating that H0 (normal, homoscedastic residuals) should be rejected. The final two columns present the β coefficients for each month to revert from JMF probability to precipitation (Subsection 3.2).

Table 4
Event (one day) correlation statistics.

Study area	Event	Kendall's tau	
		Radar	JMF
North	Dec. 7, 2018	0.33	0.38
North	Jan. 16, 2019	0.32	0.50
South	Oct. 25, 2018	0.60	0.61

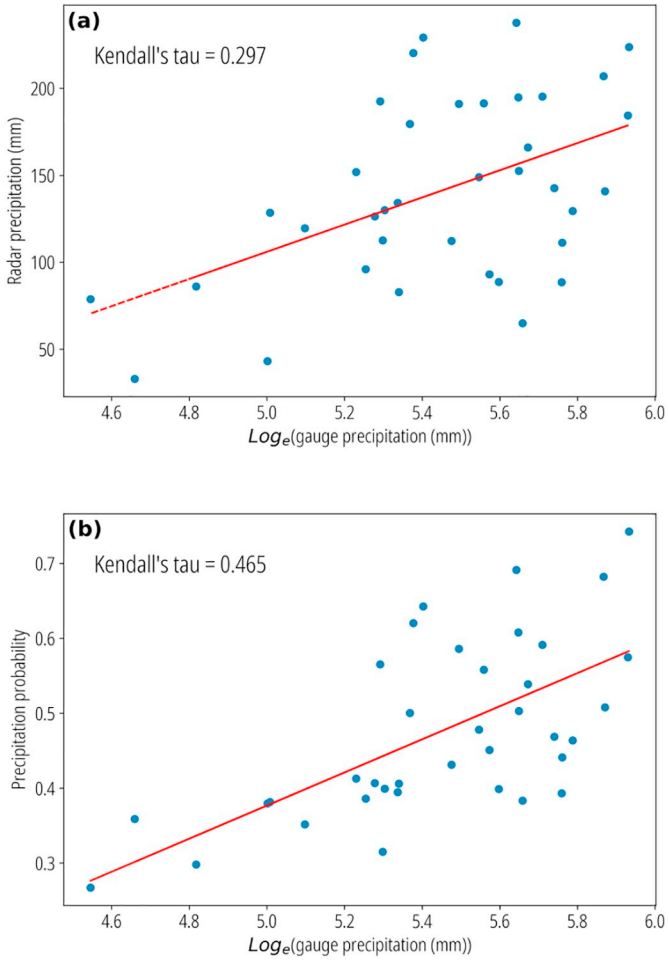

Fig. 4. Scatter plots of radar precipitation (a) and joint membership probability (b) vs. log of gauge observed precipitation, North region, 01/2018.

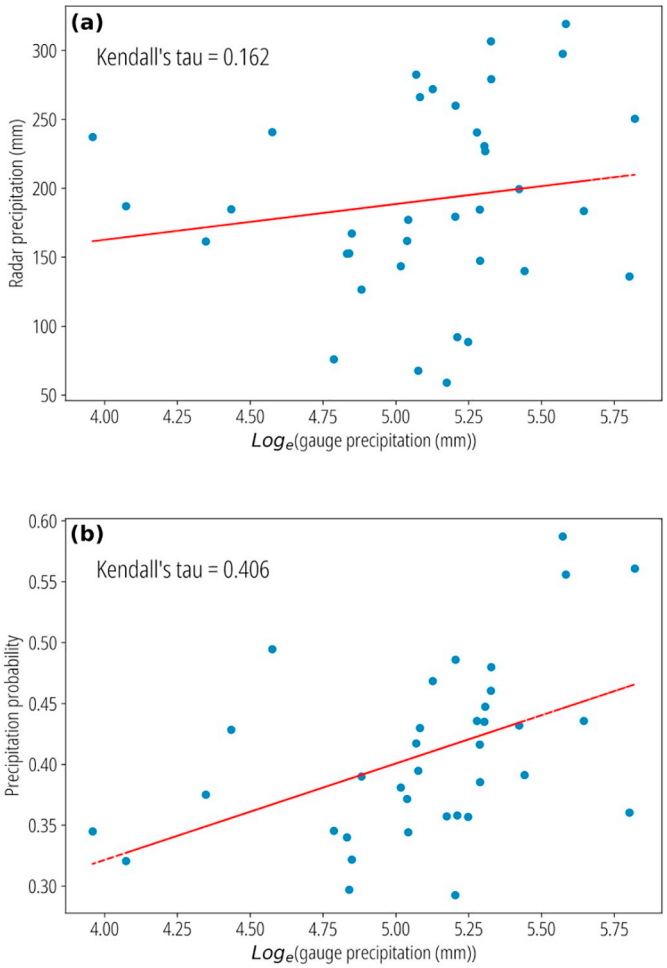

Fig. 5. Scatter plots of radar precipitation (a) and joint membership probability (b) vs. log of gauge observed precipitation, North region, 01/2019.

success (see Section 3). The specific 24 hour periods were chosen to overlap with heavy storm events: October 25, 2018; December 7, 2018; January 16, 2019 to produce JMF probability grids for these individual storms (refer to Section 1.4).

2.4. Validation

Using the gauge locations (see Section 2.1), pixel values from both the radar grids and the JMF probability grids were extracted. In both

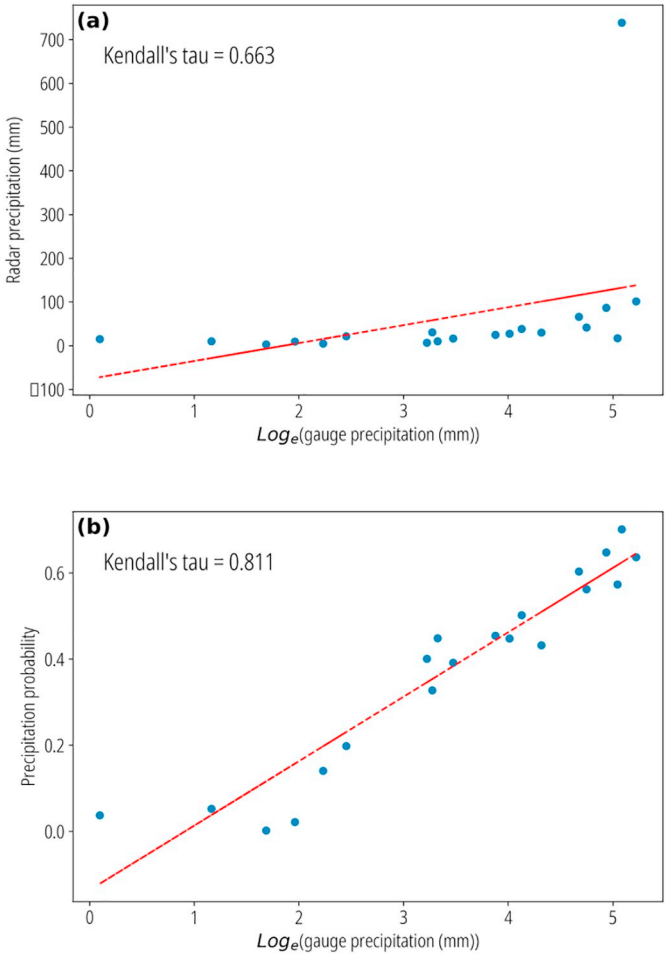

Fig. 6. Scatter plots of radar precipitation (a) and joint membership probability (b) vs. log of gauge observed precipitation, South region, 01/2018.

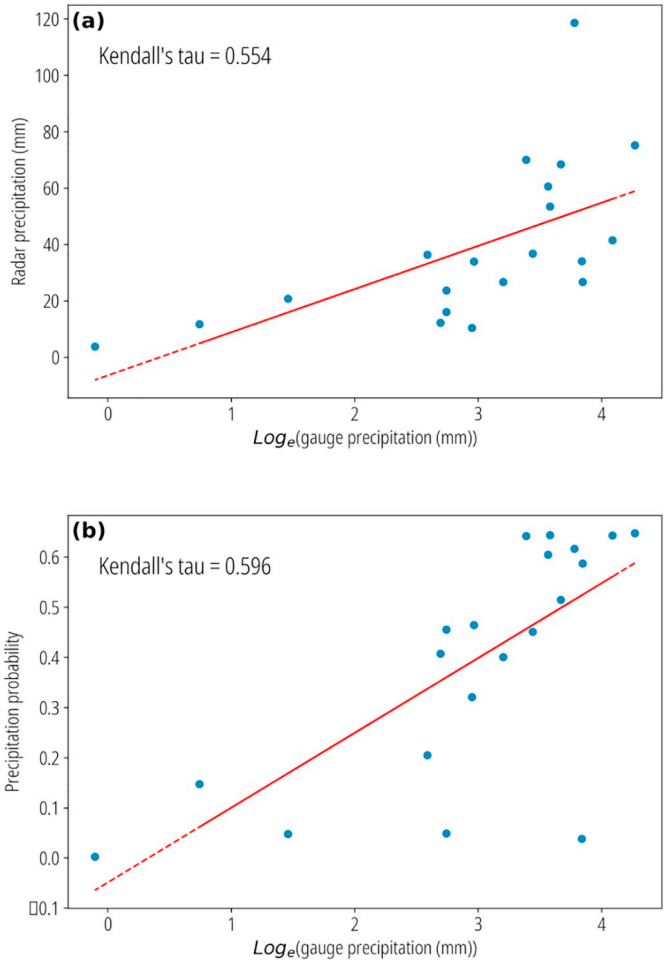

Fig. 7. Scatter plots of radar precipitation (a) and joint membership probability (b) vs. log of gauge observed precipitation, South region, 11/2018.

cases the values from four pixels surrounding the gauge location were averaged to overcome local inconsistencies in the probability grid. This resulted in monthly datasets each with pairs of gauge observations/radar precipitations and gauge observations/JMF probabilities. A linear regression was performed on each of the pairs for each monthly dataset, and for the north and south study areas separately.

With the small sample size available ($N = 37$ and $N = 20$ in the north and south study areas respectively) concern arose that the coefficient of determination would not be a reliable test of correlation due to non-normal distribution of residuals or heteroscedasticity. Residual plots were examined (see Fig. 3), and two tests performed: Shapiro-Wilk to check for normality of residuals, and Breusch-Pagan to check for heteroscedasticity. When either of these tests resulted in a $p-$ value < 0.05, then that served as evidence to reject the null hypothesis (H0 assumes normal and homoscedastic), and parametric correlation tests such as Pearson should be avoided. One or the other of these tests did suggest rejecting the null hypothesis, and examination of the residuals and QQ-plots confirmed the suspicion. Therefore the non-parametric Kendall's tau test for correlation was chosen instead. Correlation results appear in Table 3 for the monthly aggregations, and Table 4 for individual storm events with 24 hour aggregations. The left column of the Kendall's tau statistic refers to gauges and the radar grid, and the second column refers to correlation between gauges and the JMF probability grid (both at gauge locations).

3. Results

Once the fuzzy set framework was constructed and validated, two collections of results were produced: scatter plots and precipitation maps. Both were prepared in pairs, on one hand the gauge data compared to radar precipitation and on the other hand gauge data compared to the JMF derived precipitation.

3.1. Scatter plots

Initially, gauge precipitation values were plotted against the JMF probability at gauge locations (averaging four pixels around each gauge location in the JMF grid). Examining these initial graphs, it became clear that the correlation between gauge data and the JMF probability was best matched on a log scale. This was expected since four of the MF probability curves were prepared (see Section 2.2 and Eq. (3)) as functions of $\sin^2$, suggesting that a best fit linear regression would be obtained using an exponential scale. Therefore all further correlations compared radar or JMF precipitation grids to log_e of the gauge observations.

Referring to the scatter plots in Figs. 4 to 8 this choice of a log scale for the gauge observations proved to be correct. Each pair of graphs presents the results for one monthly aggregation, in panels (a) the original radar vs log_e of gauge observations, and panels (b) represent the JMF probability vs. log_e of the gauges. The blue points on all panel (b) graphs, JMF probability values, show a fairly good fit to the linear regression line. Scatter plots are presented for two months in the northern region and three months in the southern region. Results for other months appear in Table 3.

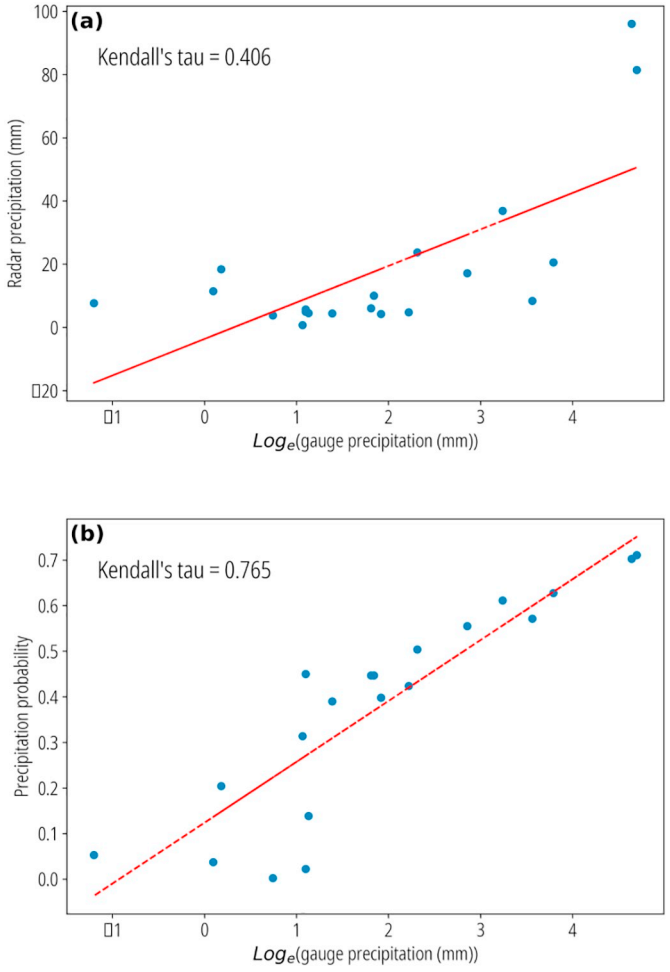

Fig. 8. Scatter plots of radar precipitation (a) and joint membership probability (b) vs. log of gauge observed precipitation, South region, 12/2018.

3.2. Precipitation maps

Next, the linear regression coefficients, β_1 (the regression rate of change) and β_0 (the regression intercept), were extracted for each month and study region, and were applied to the JMF probability grids to reconstruct the final JMF precipitation grids. These coefficients appear in Table 3. Since the linear regression was applied to log_e of the gauge values, the equation to reconstruct the JMF predicted precipitation grid was:

$$JMF_{precip} = e^{\left[\frac{JMF_{prob} - \beta_0}{\beta_1}\right]} \quad (4)$$

Eq. (4) produced JMF predicted precipitation grids for each month and region in the study. Figs. 9 to 12 present the radar based precipitation in panels (a) and the reconstructed JMF precipitation in panels (b) for two months in both north and south regions.

3.3. Single storm events

Also presented, in Table 4, are fuzzy model results from three 24 hour periods: October 25, 2018, December 7, 2018 and January 16, 2019, covering three storm events. The pair of scatter plots for January 16, 2019 appears in Fig. 13 and the accompanying precipitation maps in Fig. 14.

4. Discussion

4.1. Fuzzy method

This work produced improved precipitation maps from weather radar by applying a fuzzy logic model using a set of location-based variables. Choice of this modeling framework allowed flexibility in determining the spatial distribution of each variable (refer to Section 2.2). The elevation MF, for example, was not represented by the simple above sea level value. Rather a probability function assigned graduated probabilities to the range of elevations, such that all low lying areas were represented by very low probability, and all mountainous areas by high probability. In this way, the model enhanced the effect of the elevation variable. Similarly, the distance from the coast MF was chosen such that all areas within 100 km of the coast were assigned high probability, and all distant regions near zero probability, reflecting the reality of the influence of distance from the sea in the eastern Mediterranean.

The fuzzy logic approach also enabled adoption of synoptic classifications of storm events that would not have been possible in other models. The MF for aspect allowed transformation of the aspect azimuth to storm facing slopes. For each month in the study period, the proportion of each synoptic class was tallied. Then, we determined the direction of storm motion for each synoptic class, and matched that with aspect azimuth to find storm facing pixels. Each pixel was assigned a probability, derived from the proportion of synoptic events moving towards the pixel aspect. The results showed that this variable had only a minor influence on the precipitation outcome, nevertheless that level of influence in itself was appended to our composite of conclusions.

The original weather radar grids were also transformed by the radar MF to monthly probability grids. In defining the radar MF as an "S" curve, with very low probability at low rain depth, the model suppressed the misleading effects of radar uncertainty at those low rain depth areas. Furthermore, at areas of high radar precipitation, the radar MF reached probability of 1.0, thus enhancing areas where the radar grids were more likely to be reliable.

4.2. Location-based variables

With the chosen set of location-based variables, and assigned MFs, a JMF was proposed (Section 2.3 and Eq. (3)) as a sum of the MFs, each multiplied by a weight. The vector of weights was determined by running an optimization function to find the maximum correlation between gauge observations and the JMF probabilities at gauge locations. The optimization function output essentially represented the influence of each variable in the model. We found that, along with the original radar grids, distance from the coast had the greatest influence in determining high correlation with gauge observations. This was true especially in the south, where the study area reached 200 km from the coast.

The elevation MF was found to have a moderate influence in both northern and southern regions. Our result aligns well with earlier research pointing to the correlation between elevation and rainfall (Tang et al. (2018) and Lassegues (2018) are two recent examples). It is interesting to note that we found slope and aspect had a minor influence, and only in the southern study area, with an arid climate. Often slope and aspect are highly correlated with elevation, so keeping both variables in a modeling framework might lead to over-fitting. However in this case we found that slope and aspect had a minor impact only in the southern region and no impact in the northern area, therefore that concern of over-fitting could be put aside.

We associate the slight influence of slope and aspect in the arid region with rainfall depth. Storms in the southern study area are often highly convective, fast moving from the south, and with an intense rain

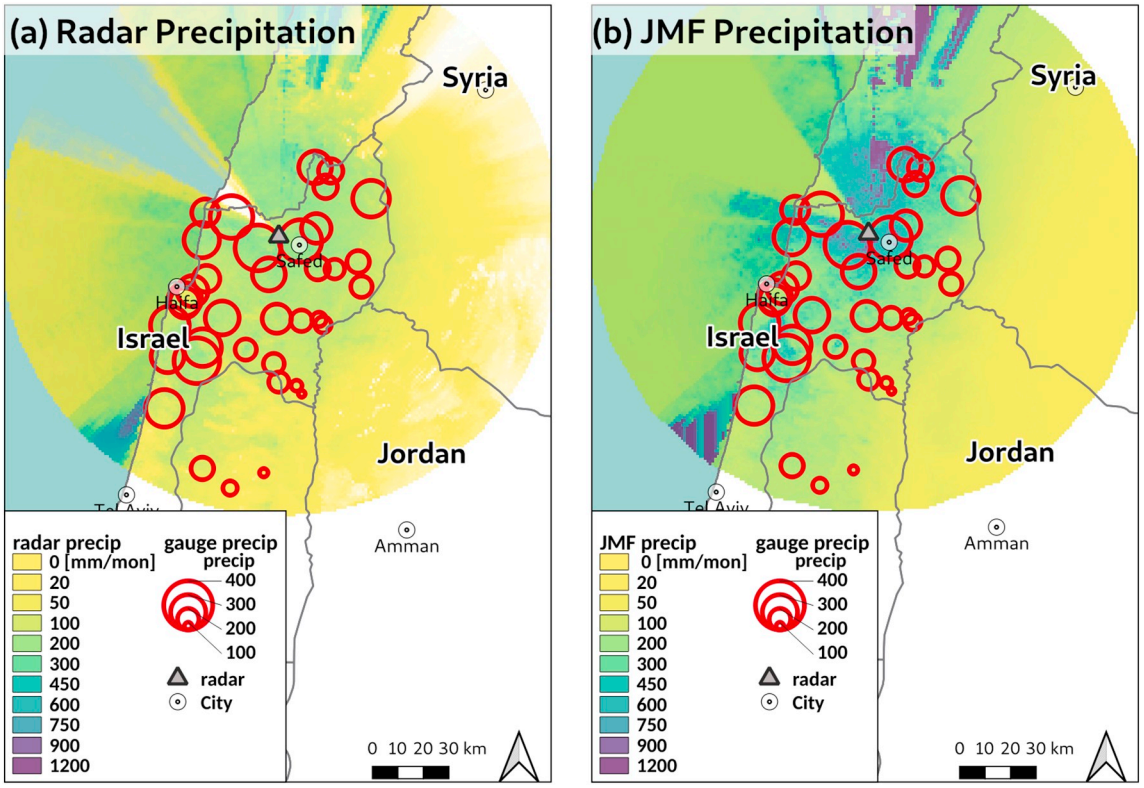

Fig. 9. Precipitation maps, radar (a) and joint membership (b) precipitation distributions, North region, 01/2018.

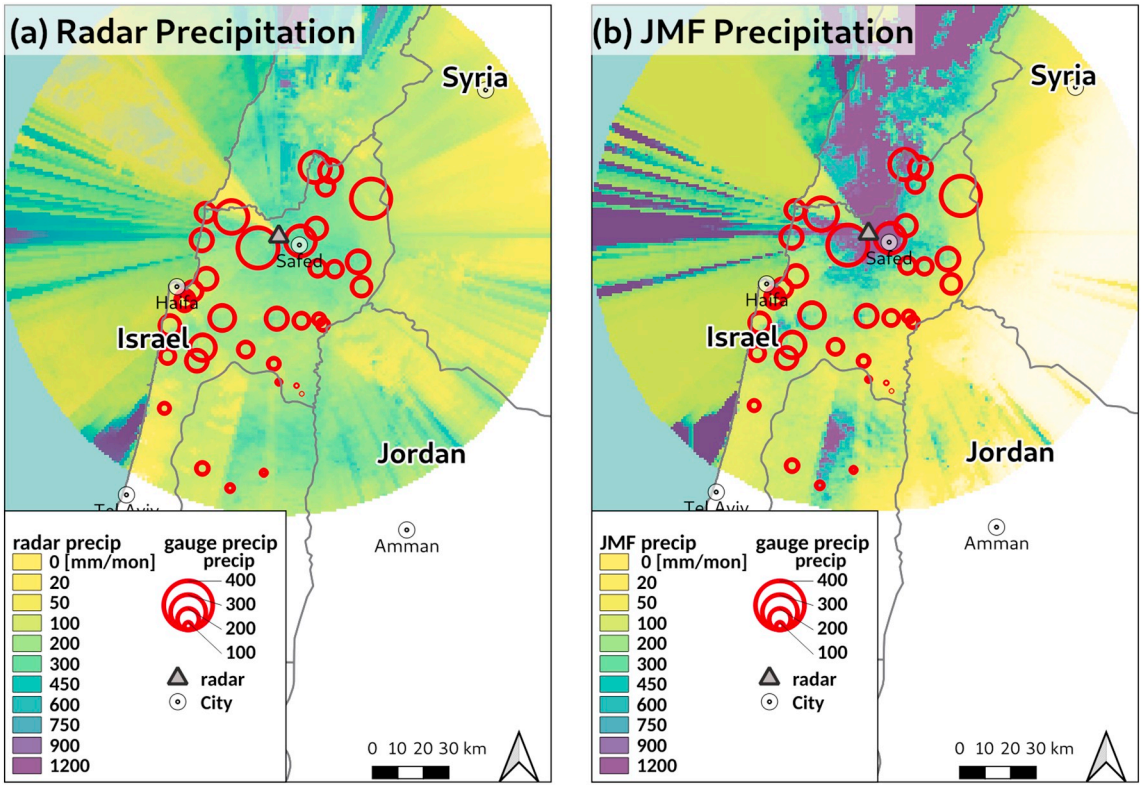

Fig. 10. Precipitation maps, radar (a) and joint membership (b) precipitation distributions, North region, 01/2019.

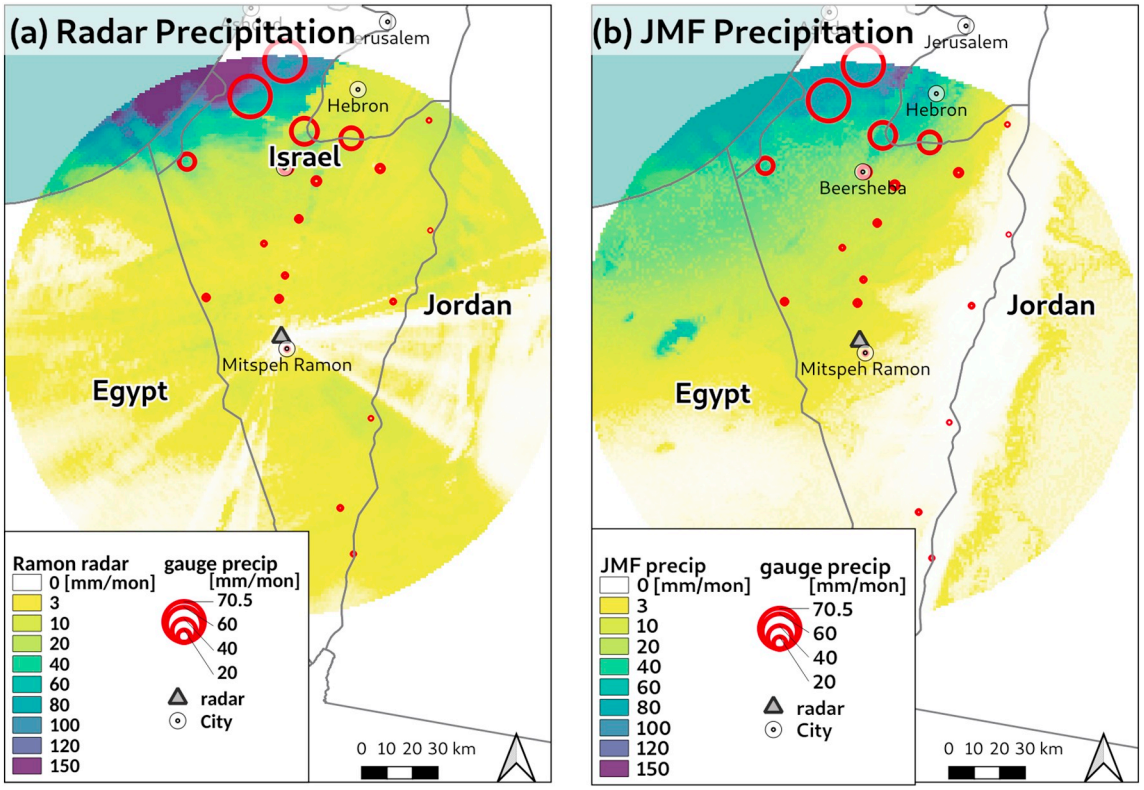

Fig. 11. Precipitation maps, radar (a) and joint membership (b) precipitation distributions, South region, 12/2018.

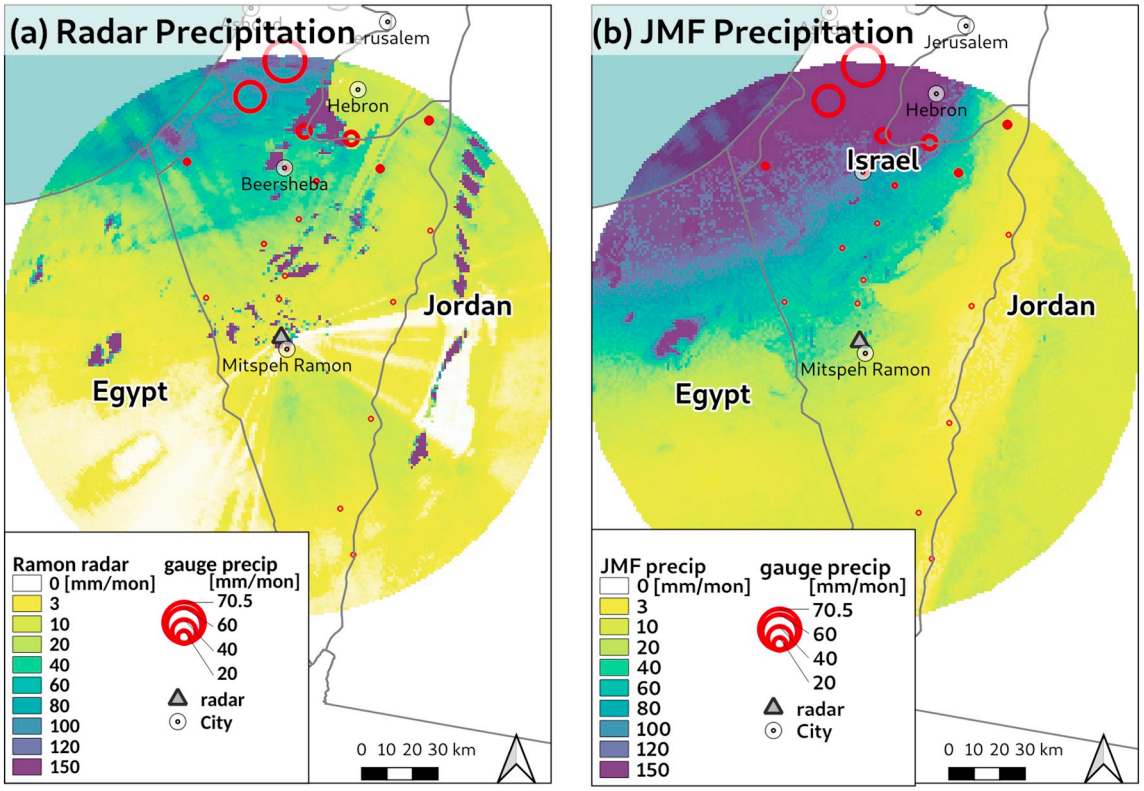

Fig. 12. Precipitation maps, radar (a) and joint membership (b) precipitation distributions, South region, 01/2019.

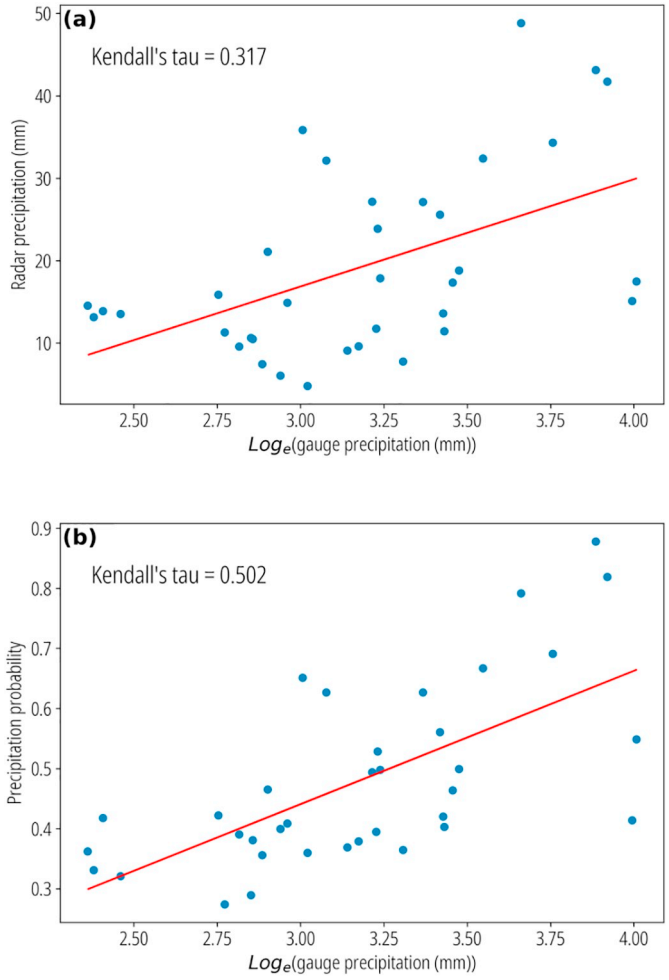

Fig. 13. Single storm event scatter plots of radar precipitation (a) and joint membership probability (b) vs. log of gauge observed precipitation, North region, 16/01/2019.

rate for a short time, but small total rainfall depth. In these cases both slope and aspect have some impact, due to orographic forcing. In the northern study area, conversely, storms are often classified as a Cyprus low front, which moves more slowly, and releases heavy precipitation over longer periods. In that case, neither slope nor aspect influence the rain depth as precipitation is released throughout the mountain areas.

A small number of papers, as far as the authors are aware, have examined the effect of slope or aspect on precipitation, Sanchez-Moreno et al. (2014) being one example. However that work was done on an island, with very unique weather behavior. Kitchen et al. (1994), in their work on correcting weather radar for bright band effects, pointed to wind direction and speed as factors insofar as they influence orographic forcing. They refer back to Hill (1983) who reported higher rainfall over hills due to orographic effects and analyzed wind direction in this context. These previous works notwithstanding, inclusion of slope and aspect in the current work constitutes an innovation. Furthermore, the collection of location-based variables examined here has not, to the best of our knowledge, been examined together before. Most research in modeling precipitation chooses meteorological variables, and possibly elevation, as secondary inputs to geostatistic procedures such as kriging with external drift. This research merges several location-based variables that, as seen in the JMF weights, influence precipitation, and allow the model to improve weather radar precipitation grids.

4.3. Improved precipitation maps

Reviewing the correlation results in Table 3, certain months show improvement: i.e. January 2018, and December 2018. Contrary to those months, October and November stand out with little improvement and in one case (October 2018) lower correlation after applying the fuzzy model. We attribute the poor performance of the model for certain months to high localized rainfall variance over the month. The location-based based model cannot deal with extreme rainfall variance at given locations over an aggregation period. Since the variables are all spatially based, if rainfall changes dramatically over the aggregation period, at a certain location, the model fails. This limitation is revealed in the eastern Mediterranean during transition seasons such as October–November and March–April. During these months rainfall variance at each gauge can be much larger than the mean precipitation for the month, confounding this location-based based model.

To test this hypothesis, the mean (μ) and standard deviation (σ) of gauge observed precipitation for each month at the individual validation gauges were obtained. Then the coefficient of variation (CV) ($CV = \sigma/\mu$) was calculated. Average CV of all gauges for the study periods are presented in Table 5:

The high coefficient of variation (averaged over all gauges) during November 2018 in the northern region revealed that during that month there were erratic rainfall depths throughout the month, unrelated to elevation, distance from the coast, etc., thus explaining the poor correlation of the model for this month (in Table 3). This result highlighted a limitation of the location-based based model: the model is appropriate for “well-behaved” aggregation periods, i.e. periods when precipitation has a low coefficient of variation.

For those months showing improved precipitation maps, it is worthwhile to point out specific regions where the precipitation grid improved, and postulate the reason for the improvement. Referring to the pair of maps in Fig. 9 for January 2018, in the north, it is clear from the uniform size of the blue, circular gauge markers that the monthly precipitation was heavy throughout the center of this study area for that month. However the radar (panel (a)) does not correctly capture that uniform distribution. Some regions far from the radar, in the high elevation to the north east and in the southern edge are light green to yellow (low rainfall depth). The improved JMF precipitation grid, in the right panel does show increased rain depth both in the center and north, probably due to high elevation in both of these areas, and captured by the elevation MF.

Similarly, in Fig. 12 gauges at the northern edge of the southern study area, close to the coast, show fairly high precipitation for the month. The radar image incorrectly shows this area as light green. The JMF precipitation grid, however, corrects the rain depth, showing this area as dark-green to blue. The correction is most likely due to the proximity to the sea, encapsulated in the distance to coast MF.

4.4. Applicability

Flood forecasting requires highly accurate precipitation grids that can be input into a hydro-meteorological model in real time. The variables included in the fuzzy logic model proposed here can all be made available in advance or in real time. The static location-based factors are prepared once in advance. Even though the aspect variable varies month by month, dependent on the proportion of synoptic classes, those proportions, as described in Section 2.2, are available from past research. Thus the aspect MF can also be prepared in advance for all months of the year. The only varying component of the model is the weather radar grid. Outputs from weather radar are often available publicly and in real time from many national meteorological services. Therefore the option to run the proposed model and produce improved precipitation grids in real time is operationally possible.

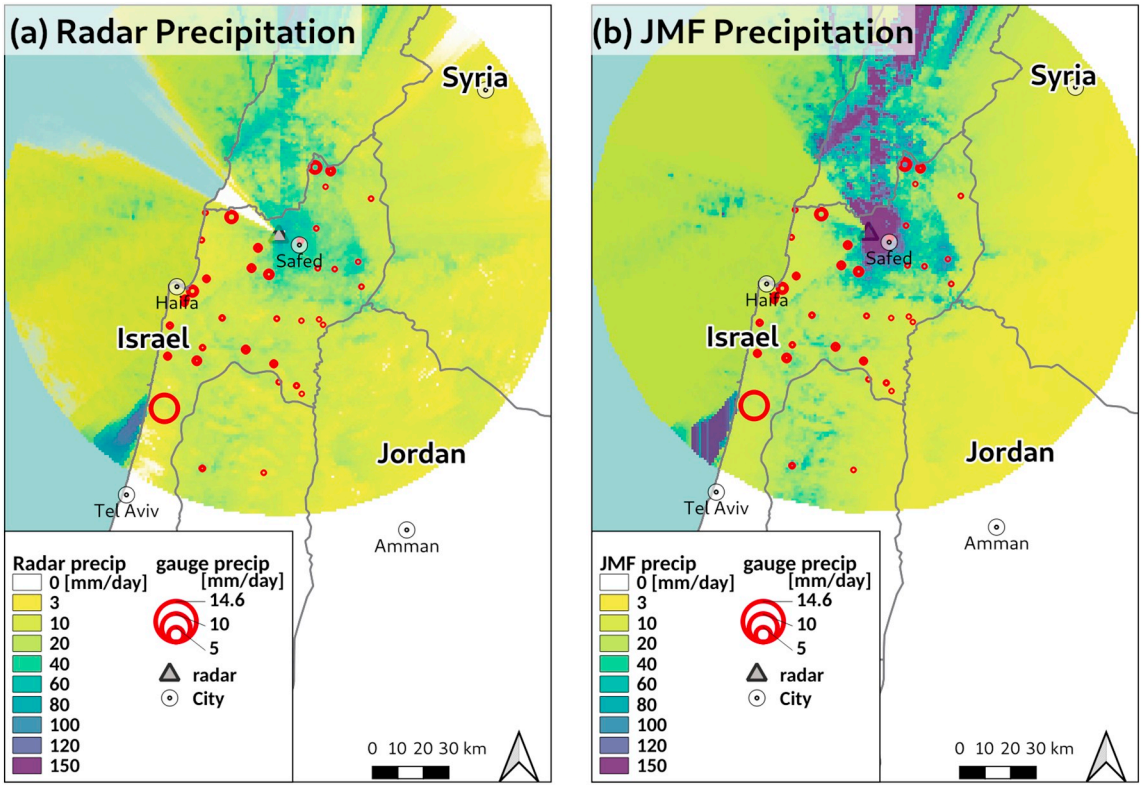

Fig. 14. Single storm event precipitation maps, radar precipitation (a) and joint membership probability (b), North region, 16/01/2019.

Table 5
Average coefficient of variation for the study periods.

Study area	Month	CV
North	Nov. 2018	**1.46**
North	Dec. 2018	1.29
North	Jan. 2019	0.89
South	Jan. 2018	1.04
South	Nov. 2018	1.24
South	Dec. 2018	1.09

The **bold cell** emphasizes a study period with high localized rainfall variance.

5. Conclusion

The fuzzy logic approach presented herein successfully produced spatially distributed precipitation grids from weather radar and location-based variables alone. The method was applied to two eastern Mediterranean study regions, over four winter months, and at both monthly and daily aggregation periods. Four variables were merged with the radar precipitation grid: elevation, distance from coast, slope and aspect. Each of these variables was expressed as a MF probability. Then a JMF of additive terms was applied, where each term was the product of one variable probability multiplied by its weight coefficient. This JMF produced precipitation probability grids for both study regions. Gauge observations from 57 locations throughout the study regions served to validate the model results.

Our finds indicate:

1. The JMF derived precipitation grids were better correlated to gauge observations than the original radar;
2. JMF probabilities were linearly correlated to log_e of the gauge observations;
3. The two most influential variables were distance from the coast and the original weather radar grid;
4. Elevation had a moderate influence in both climate regions;
5. Slope and aspect (storm facing slopes) had a minor influence only in the southern arid region;
6. The model performed poorly during aggregation periods when precipitation displayed a high localized coefficient of variation.

Declaration of Competing Interest

The authors declare that they have no known competing financial interests or personal relationships that could have appeared to influence the work reported in this paper.

Acknowledgements

The authors thank the Israeli Meteorological Service for their effort in offering public access to their climate data. We also thank Dr. Nir Sapir from the University of Haifa, Department of Evolutionary and Environmental Biology, and his research staff for their help in obtaining the radar data files.

This research was partially funded by DFG/IMAP grant GZ: KU2090/7-2, AOBJ: 633213.

References

Adhikary, S.K., Muttil, N., Yilmaz, A.G., 2017. Cokriging for enhanced spatial interpolation of rainfall in two Australian catchments. Hydrol. Process. 31, 2143–2161. URL. http://doi.wiley.com/10.1002/hyp.11163,. https://doi.org/10.1002/hyp.11163.

Agboola, A., Gabriel, A., Aliyu, E., Alese, B., 2015. Development of a fuzzy logic based rainfall prediction model. Int. J. Eng. Technol. 3.

Alpert, P., Osetinsky, I., Ziv, B., Shafir, H., 2004. Semi-objective classification for daily synoptic systems: application to the eastern mediterranean climate change. Int. J. Climatol. 24, 1001–1011. URL. http://doi.wiley.com/10.1002/joc.1036. https://doi.org/10.1002/joc.1036.

Arazi, A., Sharon, D., Khain, A., Huss, A., Mahrer, Y., 1997. The windfield and rainfall distribution induced within a small valley: field observations and 2-d numerical modelling. Bound.-Layer Meteorol. 83, 349–374. URL. http://link.springer.com/10.1023/A:1000243312103. https://doi.org/10.1023/A:1000243312103.

Asklany, S.A., Elhelow, K., Youssef, I., Abd El-wahab, M., 2011. Rainfall events prediction

using rule-based fuzzy inference system. Atmos. Res. 101, 228–236. URL. http://linkinghub.elsevier.com/retrieve/pii/S0169809511000640. https://doi.org/10.1016/j.atmosres.2011.02.015.
Berenguer, M., Sempere-Torres, D., Corral, C., Sánchez-Diezma, R., 2006. A Fuzzy Logic Technique for Identifying Nonprecipitating Echoes in Radar Scans. J. Atmos. Ocean. Technol. 23, 1157–1180. URL. http://journals.ametsoc.org/doi/abs/10.1175/JTECH1914.1. https://doi.org/10.1175/JTECH1914.1.
Berndt, C., Rabiei, E., Haberlandt, U., 2014. Geostatistical merging of rain gauge and radar data for high temporal resolutions and various station density scenarios. J. Hydrol. 508, 88–101. URL. http://linkinghub.elsevier.com/retrieve/pii/S0022169413007476. https://doi.org/10.1016/j.jhydrol.2013.10.028.
Besalatpour, A., Hajabbasi, M.A., Ayoubi, S., Afyuni, M., Jalalian, A., Schulin, R., 2012. Soil shear strength prediction using intelligent systems: artificial neural networks and an adaptive neuro-fuzzy inference system. Soil Sci. Plant Nutr. 58, 149–160. URL. http://www.tandfonline.com/doi/abs/10.1080/00380768.2012.661078. https://doi.org/10.1080/00380768.2012.661078.
Carrera-Hernández, J., Gaskin, S., 2007. Spatio temporal analysis of daily precipitation and temperature in the Basin of Mexico. J. Hydrol. 336, 231–249. URL. http://linkinghub.elsevier.com/retrieve/pii/S0022169406006718. https://doi.org/10.1016/j.jhydrol.2006.12.021.
Cecinati, F., Rico-Ramirez, M.A., Heuvelink, G.B., Han, D., 2017. Representing radar rainfall uncertainty with ensembles based on a time-variant geostatistical error modelling approach. J. Hydrol. 548, 391–405. URL. http://linkinghub.elsevier.com/retrieve/pii/S0022169417301324. https://doi.org/10.1016/j.jhydrol.2017.02.053.
Chumchean, S., Sharma, A., Seed, A., 2003. Radar rainfall error variance and its impact on radar rainfall calibration. Phys. Chem. Earth Parts A B C 28, 27–39. URL. http://linkinghub.elsevier.com/retrieve/pii/S1474706503000056. https://doi.org/10.1016/S1474-7065(03)00005-6.
Cohen, S., Svoray, T., Laronne, J.B., Alexandrov, Y., 2008. Fuzzy-based dynamic soil erosion model (FuDSEM): modelling approach and preliminary evaluation. J. Hydrol. 356, 185–198. URL. http://linkinghub.elsevier.com/retrieve/pii/S0022169408001820. https://doi.org/10.1016/j.jhydrol.2008.04.010.
Colli, M., Lanza, L., La Barbera, P., 2013. Performance of a weighing rain gauge under laboratory simulated time-varying reference rainfall rates. Atmos. Res. 131, 3–12. URL. http://linkinghub.elsevier.com/retrieve/pii/S016980951300121X. https://doi.org/10.1016/j.atmosres.2013.04.006.
Comber, A., Fisher, P., Brunsdon, C., Khmag, A., 2012. Spatial analysis of remote sensing image classification accuracy. Remote Sens. Environ. 127, 237–246. URL. http://linkinghub.elsevier.com/retrieve/pii/S0034425712003598. https://doi.org/10.1016/j.rse.2012.09.005.
Daly, C., Neilson, R., Phillips, D., 1992. A Statistical-Topographic Model for Mapping Climatological Precipitation over Mountainous Terrain. J. Appl. Meteorol. 33, 140–158. URL. https://journals.ametsoc.org/doi/pdf/10.1175/1520-0450%281994%29033%3C0140%3AASTMFM%3E2.0.CO%3B2.
Daniels, E.E., Lenderink, G., Hutjes, R.W.A., Holtslag, A.A.M., 2014. Spatial precipitation patterns and trends in the Netherlands during 1951-2009: spatial precipitation patterns and trends. Int. J. Climatol. 34, 1773–1784. URL. http://doi.wiley.com/10.1002/joc.3800. https://doi.org/10.1002/joc.3800.
Dieulin, C., Mahé, G., Paturel, J.E., Ejjiyar, S., Tramblay, Y., Rouché, N., EL Mansouri, B., 2019. A New 60-year 1940/1999 monthly-gridded rainfall data set for Africa. Water 11, 387. URL. http://www.mdpi.com/2073-4441/11/2/387. https://doi.org/10.3390/w11020387.
Dufton, D.R.L., Collier, C.G., 2015. Fuzzy logic filtering of radar reflectivity to remove nonmeteorological echoes using dual polarization radar moments. Atmos. Meas. Tech. 8, 3985–4000. URL. https://www.atmos-meas-tech.net/8/3985/2015/. https://doi.org/10.5194/amt-8-3985-2015.
Foody, G.M., 1996. Approaches for the production and evaluation of fuzzy land cover classifications from remotely-sensed data. Int. J. Remote Sens. 17, 1317–1340. URL. http://www.tandfonline.com/doi/abs/10.1080/01431169608948706. https://doi.org/10.1080/01431169608948706.
Foody, G.M., 2002. Status of land cover classification accuracy assessment. Remote Sens. Environ. 80, 185–201. URL. http://linkinghub.elsevier.com/retrieve/pii/S0034425701002954. https://doi.org/10.1016/S0034-4257(01)00295-4.
Giap, Q.H., 2014. Interactive diagnosis for a grid network of rain gauges using fuzzy reasoning. Eng. Appl. Artif. Intell. 15.
Goovaerts, P., 2000. Geostatistical approaches for incorporating elevation into the spatial interpolation of rainfall. J. Hydrol. 228, 113–129. URL. http://linkinghub.elsevier.com/retrieve/pii/S002216940000144X. https://doi.org/10.1016/S0022-1694(00)00144-X.
Guan, H., Wilson, J.L., Makhnin, O., 2005. Geostatistical mapping of mountain precipitation incorporating autosearched effects of terrain and climatic characteristics. J. Hydrometeorol. 6, 1018–1031. URL. https://journals.ametsoc.org/doi/full/10.1175/JHM448.1. https://doi.org/10.1175/JHM448.1.
Guiffrida, A., Nagi, R., 1998. Fuzzy set theory applications in production management research: a literature survey. J. Intell. Manuf. 9, 18.
Hayward, D., Clarke, R.T., 1996. Relationship between rainfall, altitude and distance from the sea in the freetown peninsula, Sierra Leone. Hydrol. Sci. J. 41, 377–384. URL. https://www.tandfonline.com/doi/full/10.1080/02626669609491509. https://doi.org/10.1080/02626669609491509.
Heistermann, M., Jacobi, S., Pfaff, T., 2013. Technical note: an open source library for processing weather radar data (wradlib). Hydrol. Earth Syst. Sci. 17, 863–871. URL. http://www.hydrol-earth-syst-sci.net/17/863/2013/. https://doi.org/10.5194/hess-17-863-2013.
Hill, F.F., 1983. The use of average annual rainfall to derive estimates of orographic enhancement of frontal rain over England and Wales for different wind directions. J. Climatol. 3, 113–129. URL. http://doi.wiley.com/10.1002/joc.3370030202. https://doi.org/10.1002/joc.3370030202.
Hong, H., Panahi, M., Shirzadi, A., Ma, T., Liu, J., Zhu, A.X., Chen, W., Kougias, I., Kazakis, N., 2018. Flood susceptibility assessment in hengfeng area coupling adaptive neuro-fuzzy inference system with genetic algorithm and differential evolution. Sci. Total Environ. 621, 1124–1141. URL. https://linkinghub.elsevier.com/retrieve/pii/S0048969717328176. https://doi.org/10.1016/j.scitotenv.2017.10.114.
Hundecha, Y., Bardossy, A., Werner, H.W., 2001. Development of a fuzzy logic-based rainfall-runoff model. Hydrol. Sci. J. 46, 363–376. URL. http://www.tandfonline.com/doi/abs/10.1080/02626660109492832. https://doi.org/10.1080/02626660109492832.
Jang, J.S., 1993. ANFIS: adaptive-network-based fuzzy inference system. IEEE Trans. Syst. Man Cybern. 23, 665–685. URL. http://ieeexplore.ieee.org/document/256541/. https://doi.org/10.1109/21.256541.
Jasiewicz, J., 2011. A new GRASS GIS fuzzy inference system for massive data analysis. Comput. Geosci. 37, 1525–1531. URL. https://linkinghub.elsevier.com/retrieve/pii/S0098300410003171. https://doi.org/10.1016/j.cageo.2010.09.008.
Kadmon, R., Danin, A., 1999. Distribution of plant species in Israel in relation to spatial variation in rainfall. J. Veg. Sci. 10, 421–432. URL. https://onlinelibrary.wiley.com/doi/abs/10.2307/3237071. https://doi.org/10.2307/3237071.
Kebaili Bargaoui, Z., Chebbi, A., 2009. Comparison of two kriging interpolation methods applied to spatiotemporal rainfall. J. Hydrol. 365, 56–73. URL. http://linkinghub.elsevier.com/retrieve/pii/S0022169408005726. https://doi.org/10.1016/j.jhydrol.2008.11.025.
Kidd, C., Becker, A., Huffman, G.J., Muller, C.L., Joe, P., Skofronick-Jackson, G., Kirschbaum, D.B., 2017. So, how much of the Earth's Surface is Covered by rain Gauges? Bull. Am. Meteorol. Soc. 98, 69–78. URL. http://journals.ametsoc.org/doi/10.1175/BAMS-D-14-00283.1. https://doi.org/10.1175/BAMS-D-14-00283.1.
Kim, B.S., Hong, J.B., Kim, H.S., Yoon, S.Y., 2007. Combining radar and rain gauge rainfall estimates for flood forecasting using conditional merging method. Am. Soc. Civil Eng. 1–16. URL. http://ascelibrary.org/doi/10.1061/40927%28243%29414. https://doi.org/10.1061/40927(243)414.
Kirstetter, P.E., Delrieu, G., Boudevillain, B., Obled, C., 2010. Toward an error model for radar quantitative precipitation estimation in the C_evennes–vivarais region, France. J. Hydrol. 394, 28–41. URL. http://linkinghub.elsevier.com/retrieve/pii/S002216941000020X. https://doi.org/10.1016/j.jhydrol.2010.01.009.
Kitchen, M., Brown, R., Davies, A.G., 1994. Real-time correction of weather radar data for the effects of bright band, range and orographic growth in widespread precipitation. Q.J Royal Met. Soc. 120, 1231–1254. URL. http://doi.wiley.com/10.1002/qj.49712051906. https://doi.org/10.1002/qj.49712051906.
Klir, G., Yuan, B., 1995. Fuzzy Sets and Fuzzy Logic Theory and Applications. Prentice-Hall Inc URL. https://www.scribd.com/doc/50284358/Fuzzy-Sets-and-Fuzzy-Logic-Theory-and-Applications-George-j-Klir-Bo-Yuan.
Kottek, M., Grieser, J., Beck, C., Rudolf, B., Rubel, F., 2006. World map of the köppen-geiger climate classification updated. Meteorol. Z. 15, 259–263. URL. https://doi.org/10.1127/0941-2948/2006/0130. https://doi.org/10.1127/0941-2948/2006/0130.
Krajewski, W., Smith, J., 2002. Radar hydrology: rainfall estimation. Adv. Water Resour. 25, 1387–1394. URL. http://linkinghub.elsevier.com/retrieve/pii/S0309170802000623. https://doi.org/10.1016/S0309-1708(02)00062-3.
Krause, J.M., 2016. A simple algorithm to discriminate between meteorological and nonmeteorological radar echoes. J. Atmos. Ocean. Technol. 33, 1875–1885. URL. http://journals.ametsoc.org/doi/10.1175/JTECH-D-15-0239.1. https://doi.org/10.1175/JTECH-D-15-0239.1.
Lassegues, P., 2018. Daily and climatological fields of precipitation over the western Alps with a high density network for the period of 1990–2012. Theor. Appl. Climatol. 131, 1–17. URL. http://link.springer.com/10.1007/s00704-016-1954-z. https://doi.org/10.1007/s00704-016-1954-z.
Ly, S., Charles, C., Degré, A., 2013. Different methods for spatial interpolation of rainfall data for operational hydrology and hydrological modeling at watershed scale. Rev. Biotechnol. Agron. Soc. Environ. 15.
Makarieva, A.M., Gorshkov, V.G., Li, B.L., 2009. Precipitation on land versus distance from the ocean: evidence for a forest pump of atmospheric moisture. Ecol. Complex. 6, 302–307. URL. https://linkinghub.elsevier.com/retrieve/pii/S1476945X08000834. https://doi.org/10.1016/j.ecocom.2008.11.004.
Marra, F., Morin, E., 2018. Autocorrelation structure of convective rainfall in semiarid-arid climate derived from high-resolution X-Band radar estimates. Atmos. Res. 200, 126–138. URL. http://linkinghub.elsevier.com/retrieve/pii/S0169809517309936. https://doi.org/10.1016/j.atmosres.2017.09.020.
McKee, J.L., Binns, A.D., 2016. A review of gauge–radar merging methods for quantitative precipitation estimation in hydrology. Can. Water Resour. J. Rev. Can. Ressources Hydriques 41, 186–203. URL. http://www.tandfonline.com/doi/full/10.1080/07011784.2015.1064786. https://doi.org/10.1080/07011784.2015.1064786.
Men, B., Long, R., Li, Y., Liu, H., Tian, W., Wu, Z., 2017. Combined forecasting of Rainfall based on Fuzzy Clustering and Cross Entropy. Entropy 19, 694. URL. http://www.mdpi.com/1099-4300/19/12/694. https://doi.org/10.3390/e19120694.
Merz, B., Aerts, J., Arnbjerg-Nielsen, K., Baldi, M., Becker, A., Bichet, A., Blöschl, G., Bouwer, L.M., Brauer, A., Cioffi, F., Delgado, J.M., Gocht, M., Guzzetti, F., Harrigan, S., Hirschboeck, K., Kilsby, C., Kron, W., Kwon, H.H., Lall, U., Merz, R., Nissen, K., Salvatti, P., Swierczynski, T., Ulbrich, U., Viglione, A., Ward, P.J., Weiler, M., Wilhelm, B., Nied, M., 2014. Floods and climate: emerging perspectives for flood risk assessment and management. Nat. Hazards Earth Syst. Sci. 14, 1921–1942. URL.

http://www.nat-hazards-earth-syst-sci.net/14/1921/2014/. https://doi.org/10.5194/nhess-14-1921-2014.
Morin, E., Gabella, M., 2007. Radar-based quantitative precipitation estimation over Mediterranean and dry climate regimes. J. Geophys. Res. 112. URL. http://doi.wiley.com/10.1029/2006JD008206. https://doi.org/10.1029/2006JD008206.
Morin, E., Krajewski, W.F., Goodrich, D.C., Gao, X., Sorooshian, S., 2003. Estimating rainfall intensities from weather radar data: the scale-dependency problem. J. Hydrometeorol. 4, 782–797. URL. http://journals.ametsoc.org/doi/abs/10.1175/1525-7541(2003)004%3C0782:ERIFWR%3E2.0.CO%3B2.
Neteler, M., Bowman, M.H., Landa, M., Metz, M., 2012. GRASS GIS: a multi-purpose open source GIS. Environ. Model. Softw. 31, 124–130. URL. http://linkinghub.elsevier.com/retrieve/pii/S1364815211002775. https://doi.org/10.1016/j.envsoft.2011.11.014.
Ogino, S.Y., Yamanaka, M.D., Mori, S., Matsumoto, J., 2016. How much is the precipitation amount over the tropical coastal region? J. Clim. 29, 1231–1236. URL. http://journals.ametsoc.org/doi/10.1175/JCLI-D-15-0484.1. https://doi.org/10.1175/JCLI-D-15-0484.1.
Okeke, F., Karnieli, A., 2006. Methods for fuzzy classification and accuracy assessment of historical aerial photographs for vegetation change analyses. Part I: algorithm development. Int. J. Remote Sens. 27, 153–176. URL. https://www.tandfonline.com/doi/full/10.1080/01431160500166540. https://doi.org/10.1080/01431160500166540.
Otieno, H., Yang, J., Liu, W., Han, D., 2014. Influence of rain gauge density on interpolation method selection. J. Hydrol. Eng. 19, 04014024 URL. http://ascelibrary.org/doi/10.1061/%28ASCE%29HE.1943-5584.0000964. https://doi.org/10.1061/(ASCE)HE.1943-5584.0000964.
Paulat, M., Frei, C., Hagen, M., Wernli, H., 2008. A Gridded Dataset of Hourly Precipitation in Germany: Its Construction, Climatology and Application. Metz. vol. 17. pp. 719–732. URL. http://www.schweizerbart.de/papers/metz/detail/17/56817/A_gridded_dataset_of_hourly_precipitation_in_Germa?af=crossref. https://doi.org/10.1127/0941-2948/2008/0332.
Reid, I., 1973. The influence of slope aspect on precipitation receipt. Weather 28, 490–494. URL. https://rmets.onlinelibrary.wiley.com/doi/abs/10.1002/j.1477-8696.1973.tb00814.x. https://doi.org/10.1002/j.1477-8696.1973.tb00814.x.
Sanchez-Moreno, J.F., Mannaerts, C.M., Jetten, V., 2014. Influence of topography on rainfall variability in Santiago Island, Cape Verde: influence of topography on rainfall variability in cape verde. Int. J. Climatol. 34, 1081–1097. URL. http://doi.wiley.com/10.1002/joc.3747. https://doi.org/10.1002/joc.3747.
Sebastianelli, S., Russo, F., Napolitano, F., Baldini, L., 2013. On precipitation measurements collected by a weather radar and a rain gauge network. Nat. Hazards Earth Syst. Sci. 13, 605–623. URL. http://www.nat-hazards-earth-syst-sci.net/13/605/2013/. https://doi.org/10.5194/nhess-13-605-2013.
Sevruk, B., Nevenic, M., 1998. The geography and topography effects on the areal pattern of precipitation in a small prealpine basin. Water Sci. Technol. 37, 163–170. https://doi.org/10.1016/S0273-1223(98)00329-1.
Sharon, D., Arazi, A., 1997. The distribution of wind-driven rainfall in a small valley: an empirical basis for numerical model verification. J. Hydrol. 201, 21–48. URL. http://linkinghub.elsevier.com/retrieve/pii/S0022169497000346. https://doi.org/10.1016/S0022-1694(97)00034-6.
Sideris, I.V., Gabella, M., Erdin, R., Germann, U., 2014. Real-time radar-rain-gauge merging using spatio-temporal co-kriging with external drift in the alpine terrain of Switzerland: real-time radar-rain-gauge merging. Q. J. R. Meteorol. Soc. 140, 1097–1111. URL. http://doi.wiley.com/10.1002/qj.2188. https://doi.org/10.1002/qj.2188.
Sinclair, S., Pegram, G., 2005. Combining radar and rain gauge rainfall estimates using conditional merging. Atmos. Sci. Lett. 6, 19–22. http://doi.wiley.com/10.1002/asl.85 https://doi.org/10.1002/asl.85.
Sternberg, M., Shoshany, M., 2001. Influence of slope aspect on mediterranean woody formations: comparison of a semiarid and an arid site in Israel. In: Slope aspect Differences in Mediterranean woody Formations. Ecological Research. vol. 16. pp. 335–345. URL. http://doi.wiley.com/10.1046/j.1440-1703.2001.00393.x. https://doi.org/10.1046/j.1440-1703.2001.00393.x.
Svoray, T., Mazor, S., Bar Kutiel, P., 2007. How is Shrub Cover Related to Soil Moisture and Patch Geometry in the Fragmented Landscape of the Northern Negev desert? Landscape Ecol. vol. 22. pp. 105–116. URL. http://link.springer.com/10.1007/s10980-006-9004-3. https://doi.org/10.1007/s10980-006-9004-3.
Svoray, T., Shafran-Nathan, R., Henkin, Z., Perevolotsky, A., 2008. Spatially and temporally explicit modeling of conditions for primary production of annuals in dry environments. Ecol. Model. 218, 339–353. URL. http://linkinghub.elsevier.com/retrieve/pii/S0304380008003827. https://doi.org/10.1016/j.ecolmodel.2008.07.029.
Tang, G., Long, D., Hong, Y., Gao, J., Wan, W., 2018. Documentation of multifactorial relationships between precipitation and topography of the tibetan plateau using spaceborne precipitation radars. Remote Sens. Environ. 208, 82–96. URL. http://linkinghub.elsevier.com/retrieve/pii/S0034425718300130. https://doi.org/10.1016/j.rse.2018.02.007.
Todini, E., Alberoni, P., Butts, M., Collier, C., Khatibi, R., 2005. ACTIF best practice paper–understanding and reducing uncertainty in flood forecasting. In: Balabanis, P., Lumbroso, D., Samuels, P. (Eds.), International Conference on Innovation, Advances and Implementation of Flood Forecasting Technology, Troms, Norway. URL. http://www.academia.edu/download/38241880/ACTIF_best_practice_paper_1_Uncertainty_in_flood_forecasting_V2.pdf.
Villarini, G., Krajewski, W.F., 2010. Review of the different sources of uncertainty in single polarization radar-based estimates of rainfall. Surv. Geophys. 31, 107–129. URL. http://link.springer.com/10.1007/s10712-009-9079-x. https://doi.org/10.1007/s10712-009-9079-x.
Villarini, G., Mandapaka, P.V., Krajewski, W.F., Moore, R.J., 2008. Rainfall and sampling uncertainties: a rain gauge perspective. J. Geophys. Res. 113. URL. http://doi.wiley.com/10.1029/2007JD009214. https://doi.org/10.1029/2007JD009214.
Wang, X., Zheng, X., He, J., Li, X., 2012. Using fuzzy logic to discriminate convective and statiform precipitation in doppler weather radar. In: 2012 9th International Conference on Fuzzy Systems and Knowledge Discovery, pp. 623–627. https://doi.org/10.1109/FSKD.2012.6233819.
Wijitkosum, S., Sriburi, T., 2019. Fuzzy AHP Integrated with GIS Analyses for Drought Risk Assessment: A Case Study from Upper Phetchaburi River Basin. Thailand. pp. 16.
Yang, Y., Chen, X., Qi, Y., 2013. Classification of convective/stratiform echoes in radar reflectivity observations using a fuzzy logic algorithm: precipitation classification from radar. J. Geophys. Res. 118, 1896–1905. URL. http://doi.wiley.com/10.1002/jgrd.50214. https://doi.org/10.1002/jgrd.50214.
Zadeh, L.A., 1965. Fuzzy Sets. Inf. Control. 8, 338–353. URL. https://www-liphy.ujf-grenoble.fr/pagesperso/bahram/biblio/Zadeh_FuzzySetTheory_1965.pdf.
Zadeh, L.A., 1975. Fuzzy Logic and Approximate Reasoning. vol. 30. Deidel Publishing Company, pp. 22.
Zadeh, L.A., 2008. Is there a need for fuzzy logic? Inf. Sci. 178, 2751–2779. URL. http://linkinghub.elsevier.com/retrieve/pii/S0020025508000716. https://doi.org/10.1016/j.ins.2008.02.012.
Zimmermann, H.J., 2013. Fuzzy Set Theory and Its Applications. Springer Netherlands, Dordrecht URL. http://public.eblib.com/choice/publicfullrecord.aspx?p=3568591 (oCLC: 958538892).